



## Experimental investigation on the unsteady pressure pulsation of reactor coolant pumps with non-uniform inflow



Yun Long, Dezhong Wang\*, Junlian Yin, Yaoyu Hu

School of Mechanical Engineering, Shanghai Jiao Tong University, Shanghai 200240, China

### ARTICLE INFO

#### Article history:

Received 2 December 2016

Received in revised form 8 July 2017

Accepted 10 July 2017

#### Keywords:

Reactor coolant pump

Non-uniform inflow

Pressure pulsation

Experimental investigation

### ABSTRACT

In the third generation pressurized water reactor, the channel head of the steam-generator is directly connected with the reactor coolant pump. Non-uniform suction flow is generated at the inlet of the reactor coolant pump. But this situation has not been considered during the actual reactor system design process, because the pump is designed with uniform inflow. It is very necessary to conduct the research of the unsteady flow of the pump with non-uniform inflow by experiment method. Pressure pulsation signals measured from the seven sensors on the pump casing and outlet pipe are analysed by FFT and RMS method. From numerical simulation results, non-uniform inflow has a great effect on the flow structures in the pump. Pressure pulsation characteristics, both discrete peaks and RMS values, are easily affected by different operating conditions and measuring positions. Pressure amplitudes at  $f_{RPF}$  (Rotor passing frequency) and  $f_{SPF}$  (Stator passing frequency) decreases when the flow rate increases, but pressure amplitudes at  $f_R$  exhibit the contrary trend. It is found that pressure amplitudes of RMS value and  $f_{RPF}$  increase when the rotating speed increases. Nonlinear components of the frequency at the outlet could be identified easily, and more detailed analysis of the flow field need be carried out in the future. Finally, it is expected that the present work will provide a good reference for the pump design with non-uniform inflow.

© 2017 Published by Elsevier Ltd.

### 1. Introduction

The reactor coolant pump is one of the most important equipment in the nuclear power plant. In the advanced pressurized water reactor (APWR) primary coolant system, two canned motor pumps are directly attached to the cold side of the steam generator ([Sun et al., 2010](#)), as shown in [Fig. 1](#). The pumps are identical designed based on the performance under uniform inflow with the straight pipe. However actual non-uniform suction flow is generated in the discharge pipe of the steam generator due to the complex geometry in the channel head, and it would affect the pump performances ([Cheng et al., 2014](#)). Due to rotor–stator interaction, unsteady pressure pulsation has a direct impact on the stable and safe operation of pumps ([Brennen, 2011](#)). The pressure pulsations in the pump, as a boundary condition of reactor system, is also directly input to the reactor core, which affects the core security, such as the vibration of the pump and core components.

Up to now, only few researchers have studied the effect of the non-uniform inflow on the performance of the pumps. The perfor-

mance of a mixed-flow pump and hydrodynamic forces on the impeller under non-uniform suction flow are investigated with experimental method by [Van Esch \(2009\)](#), it is found that the performance of the pump is influenced by the type of suction velocity profile and a considerable steady radial force appears when the suction flow is non-uniform. The flow patterns of non-uniform flows in a rectangular open suction passage is studied using 2-D PIV method ([Xu et al., 2005](#)). The flow characteristics within the connection between the steam generator channel head and the pump suction are investigated by experimental method ([Huang et al., 2002](#)), and it is found that axial vortex is eliminated and axial velocity is uniform in the outlet section in the nozzle of the channel head. But the interaction between the channel head and the pump has not been investigated since no pumps are connected to the channel head in the test loop. The effect of the velocity distortion generated by the steam generator on the performance of the two pumps is investigated by CFD method ([Cheng et al., 2014](#)), and the results suggest that the nozzle dam brackets should be installed in the outlet pipe of the steam generator.

Generally, unsteady pressure pulsation excites mechanical vibrations of the pump even at the design operating condition. Lots of investigations have been carried out to study the unsteady flow, and fast Fourier transform (FFT) method has been proved to be the

\* Corresponding author.

E-mail addresses: [longyunjs@sjtu.edu.cn](mailto:longyunjs@sjtu.edu.cn) (Y. Long), [dzwang\\_sjtu@sina.com](mailto:dzwang_sjtu@sina.com) (D. Wang).

## Nomenclature

$D_2$	Impeller outlet diameter, 160 mm	$f_{SPF}$	Stator passing frequency, $Z_2 f_R$ , Hz
$b_2$	Impeller outlet width, 67 mm	$Z_1$	Number of impeller blade, 4
$\eta$	Efficiency	$Z_2$	Number of diffuser blade, 5
$p$	Pressure, Pa	$Q$	Nominal flow rate, 280 m <sup>3</sup> /h
$\Delta p$	Pressure changed, $\Delta p = p - \bar{A}$ , Pa	$H$	Nominal head, 6.53 m
$\bar{A}$	Mean amplitude of the pressure, Pa	$n$	Nominal Rotating speed, 1800 r/min
$\Delta H$	Pressure fluctuation described as the water column, $\Delta H = \Delta p/\rho g$ , m	$Q_{opt}$	Operational flow rate, m <sup>3</sup> /h
$\rho$	Water density, 1000 kg/m <sup>3</sup>	$H_{opt}$	Operational head, m
$f_R$	Rotating frequency of impeller blade, $n/60$ , Hz	$n_{opt}$	Operational Rotating speed, r/min
$f_{RPF}$	Rotor passing frequency, $Z_1 f_R$ , Hz	$P$	Power of the pump
		$n_s$	Specific speed, $n_s = 3.65n Q^{0.5}/H^{0.75}$ , 445.51

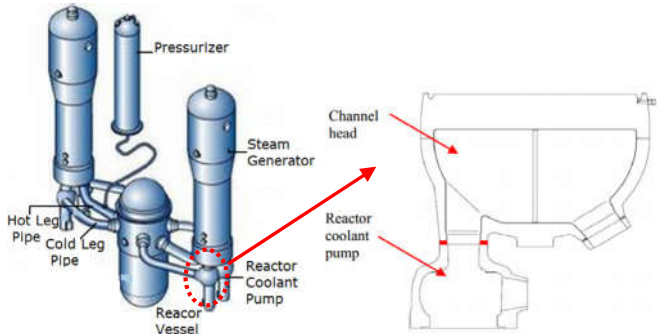


Fig. 1. Schematic diagram of connection type.

most effective tool to analyse pressure fluctuation characteristics. Both frequency domain and time-frequency domain in a double suction centrifugal pump are analysed based on FFT and time-frequency representation methods (Li et al., 2015; Yao et al., 2011). The unsteady pressure distribution in a conventional centrifugal pump are also investigated (Parrondo-Gayo et al., 2002), and they paid more attention on pressure pulsations at the blade passing frequency. Benra (2006) investigated the periodic unsteady flow in a single-blade pump by CFD simulation method and particle image velocimetry measurement method, and the results show that transient numerical simulations agree very well with velocity measurements. Pei et al. (2012, 2013) conducted the numerical investigation on the periodic unsteady flow of a single-blade pump and predicted the flow in the whole flow passage.

Under off-design conditions, some unexpected flow phenomena superposed to the rotor-stator interaction have considerable effect on vibration and safety. Toussaint (2006) conducted experimental investigation on the unsteady flow in the pump at off-design conditions and concluded that the pressure fluctuations occur at blade passing frequency, rotation frequency, and their harmonics. Barrio et al. (2008, 2010) presented a study on the fluid-dynamic pulsations and the dynamic forces in a centrifugal pump with different radial gap between the impeller and volute. They estimated the dynamic radial forces and torque at blade passing frequency, whereas the progressive reduction of the impeller-tongue gap leads to the corresponding increment in dynamic load. Wang and Tsukamoto (2003) investigated the unsteady phenomena in a diffuser pump at off-design conditions by a two-dimensional vortex method. Results showed that an asymmetrical separation bubble causes the unsteady flow near the pressure surface of the impeller vane.

Some studies focus on the influence of geometry on pressure pulsation by either experimental or numerical method. Spence and Amaral-Teixeira (2009) explored the effects of pressure pulsation

in their work, they took the form of a parametric study covering four geometric parameters by numerical analysis. And a rationalisation process aimed at reducing vibration through reductions in pressure pulsations has produced geometric recommendations. Yang et al. (2012, 2014) investigated unsteady pressure fields of the pump as turbine by numerical methods and illustrated that increasing the blade tip clearance serves as an effective measure for reducing pressure pulsation. Zhang et al. (2015) explored a slope volute pump to reduce the level of pressure pulsation and used numerical simulation to analyse its influence on flow structures.

These researchers have done a lot of work on the pressure pulsation of the pump with uniform inflow. Lots of research for the effect of pump pressure pulsation on core vibration are carried out (Cheong, 2000; Lee et al., 1992; Lee and Chandra, 1980; Penzes, 1974). However, they did not consider the effect of non-uniform inflow on pressure pulsations due to the complex geometry in the channel head of the steam-generator. Accurate pressure pulsations in the casing and outlet pipe are significant input conditions for the design of the nuclear reactor. It is very necessary to research pressure pulsations of the pumps with non-uniform inflows.

In the present study, unsteady pressure pulsation characteristics in a reactor coolant pump with channel head are investigated in various flow rates. Pressure pulsation signals are obtained with seven fast-response pressure transducers mounted on the pump casing and outlet pipe. Detailed analysis of pressure spectrum is performed by Fast Fourier Transform (FFT) method, and special attention is paid to pressure pulsation peaks at blade passing frequency and some nonlinear interaction frequency components. Meanwhile, the influence of different rotational speeds on pressure pulsation is investigated.

## 2. Model pump and experimental system

### 2.1. The model pump

The model pump was homologous to the prototype, with a diffuser in the spherical casing. The tested model pump and its structure are shown in Fig. 2. In order to guarantee a better similarity, a 1/4 scaled model pump is used for experiment. The cold side of the steam generator has two discharging pipes, as shown in Fig. 1. Since the cold side of the steam generator is symmetric, it is assumed that the flow field inside is also symmetrical. So the channel head could be divided into two mirror parts, as shown Fig. 2. The impeller has an outlet diameter of 160 mm with the other pump parameters listed in Nomenclature. The nominal flow rate  $Q = 280$  m<sup>3</sup>/h and the nominal head of the model pump  $H = 6.53$  m.

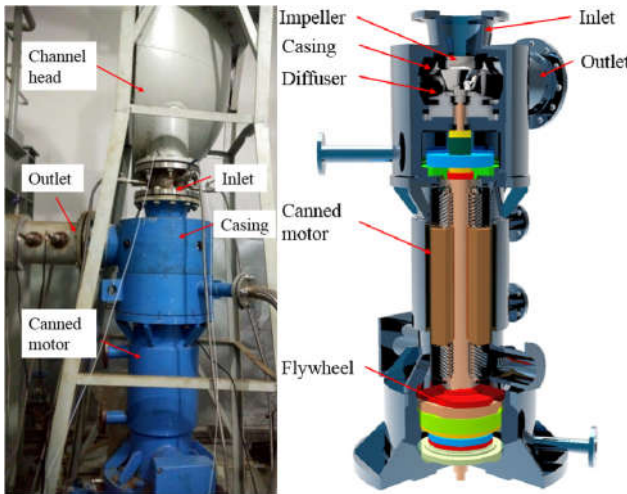


**Fig. 2.** The model pump and the structure.

## 2.2. Experimental system

A test rig is developed in order to investigate the pump hydrodynamics and pressure pulsations, as shown in Fig. 3. The tested pump is driven by a canned motor controlled by a frequency converter. The test rig is a closed circulation system equipped with calibrated equipment for various parameters including the flow rate, pressure, and power. Due to the non-uniform inflow, static pressure values are measured at the inlet and outlet of the pump by three differential pressure transducers, and the uncertainty is within  $\pm 0.065\%$ . The flow rate is measured using a magnetic flow meter with the uncertainty less than  $\pm 0.5\%$ . Piezoresistive pressure transducers with high frequency are flush mounted in the circular symmetric casing and the outlet pipe to measure the unsteady pressure signals, and the uncertainty is equal to  $\pm 0.25\%$ .

Fig. 4 presents the pump performance with uniform and non-uniform inflow at a given rotation speed of 1800 r/min. The heads of the pump with two different inflows have the similar trend at flow rates higher than  $0.5Q$ , namely the head increases with the flow rate decreasing. However, at low flow rates ( $Q_{opt} < 0.5 Q$ ), the head of the pump with uniform inflow decreases when the flow rate decreases, and the head of the pump with non-uniform inflow has an opposite trend compared with uniform inflow. Different inflows lead to the evident difference of the pump head at low flow rates. Inlet pre-swirling in the pump suction at low flow rates is the main reason of the hump of pump head curve. From the difference of the pump head with different inflows, non-uniform inflow changes flow structure at the leading edge of the blade, thus it restrains the pre-swirling in suction pipe. So the pump head curve with non-uniform inflow don't collapses. The efficiencies of the pump with two different inflows increase when the flow rate

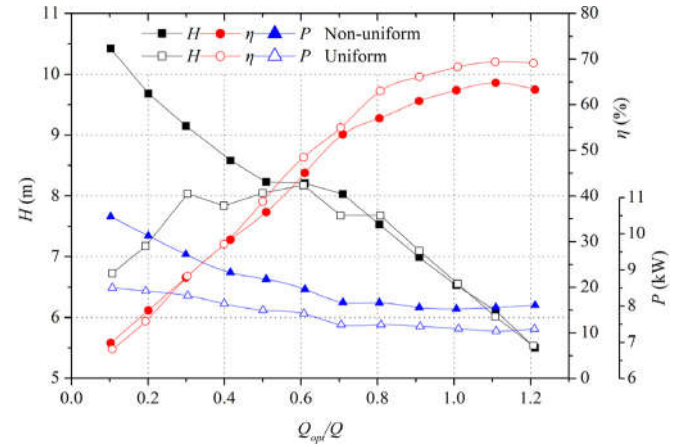


**Fig. 4.** Hydraulic characteristics of the tested pump at 1800 r/min.

increases, and the best efficiency point of the model pump is near 1.1 times of nominal flow rate. But with the flow rate increasing, the efficiency difference between non-uniform and uniform inflow increases. With the flow rate decreasing, the power of the pump with two different inflows increase, and the power difference between non-uniform and uniform inflow increases. At nominal flow rate, compared with uniform inflow, the head of the pump with non-uniform inflow decreases by 0.46%, and the efficiency of the pump with non-uniform inflow decreases by 7.5%. The power of the pump with non-uniform inflow increases by 7.32%. In conclusion, non-uniform inflow has a great effect on the pump performance.

The investigation focuses on pressure fluctuations in the outlet pipe and the pump casing caused by hydraulic excitations when the suction flow of the pump is non-uniform. Pressure pulsation signals were measured by seven transducers, four mounted on the pump casing (P1, P2, P3, P4) and three on the outlet pipe (P5, P6, P7), as shown in Fig. 5. The signals were acquired with a sampling rate of 8 kHz and a sampling time of 5 s.

## 3. Results and discussions

### 3.1. Influence of the Non-uniform inflow on flow structures within the model pump

To clarify the influence of the non-uniform inflow on the hydraulic dynamic characteristics, it is necessary to analyse the flow structures in the pump. The three-dimensional pump internal flow channel was modelled by pro/E software, and Reynolds-averaged Naiver-Stokes equations with the  $k - \epsilon$  turbulence model were solved by the computational fluid dynamics software CFX to conduct the steady numerical simulation. The mass flow rate at inlet and the pressure at outlet are set as the boundary conditions.

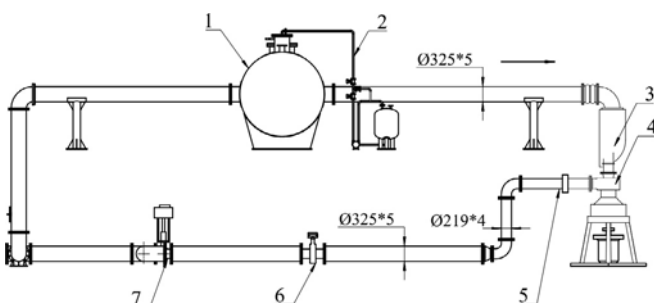


**Fig. 3.** Closed-circulation experimental system for the model pump.

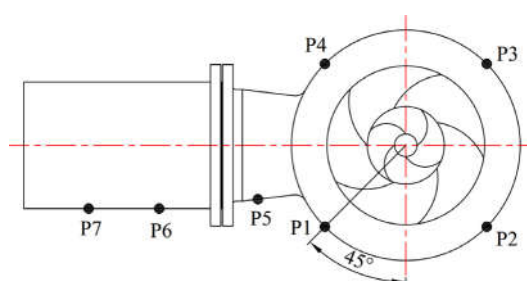


**Fig. 5.** Positions of pressure transducers.

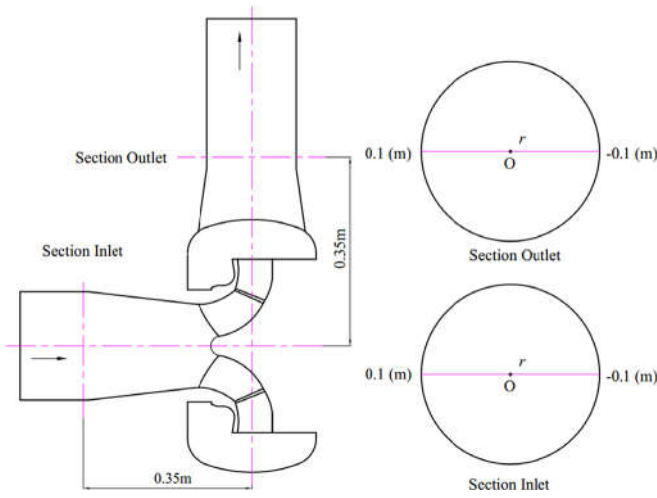


Fig. 6. The section selected for flow analysis.

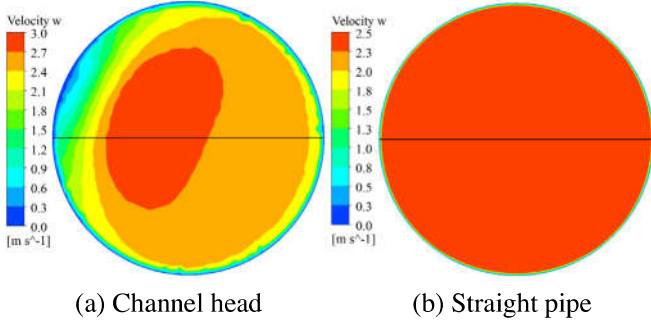


Fig. 7. Axial velocity at Section Inlet.

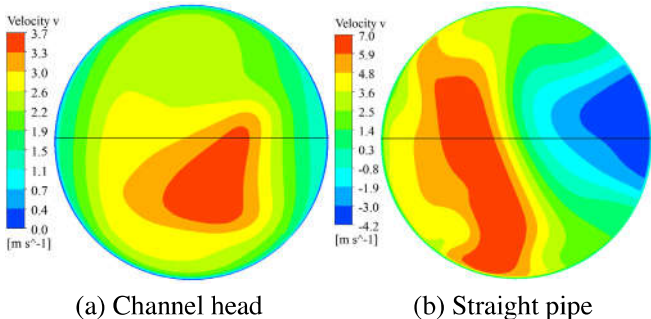


Fig. 8. Axial velocity at Section Outlet.

Fig. 6 shows the section selected for flow analysis. Section Inlet is the section at 0.35 m from the axis of the outlet pipe, and Section Outlet is the section at 0.35 m from the axis of the inlet pipe. Fig. 7 presents a comparison of velocity distributions on Section Inlet of different inflows at the nominal flow rate. The axial velocity with channel head is lower at left of Section Inlet, and the axial velocity with straight pipe is uniform on the whole Section Inlet. Therefore, it is concluded that the complex geometry of the channel head leads to the non-uniform inflow. Fig. 8 presents a comparison of velocity distributions on Section Outlet of different inflows at the nominal flow rate. It is observed that flow patterns at Section Outlet of the pump with two different inflows are obviously different. The high velocity at the Section Outlet of the pump with channel head is at the underneath, and the high

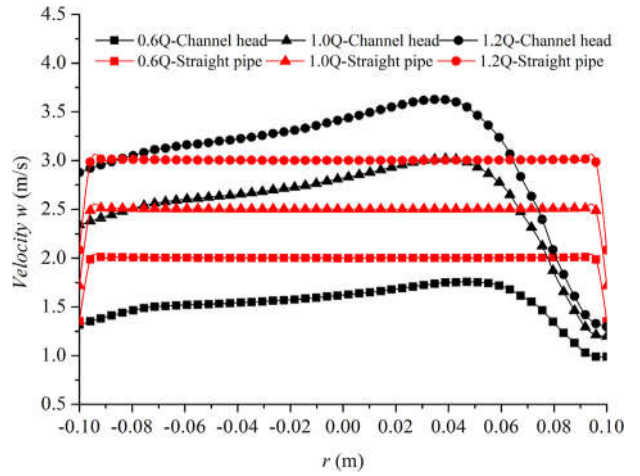


Fig. 9. The axial velocity of the line on Section Inlet.

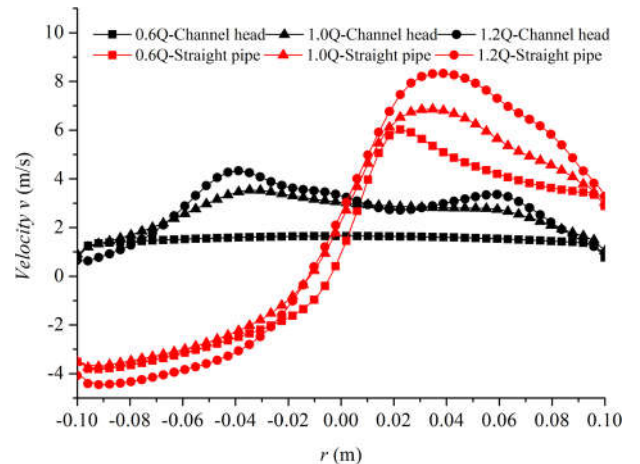


Fig. 10. The axial velocity of the line on Section Outlet.

velocity at the Section Outlet of the pump with straight pipe is at the left. The negative velocity is at the right of Section Outlet with straight pipe inflow. Therefore, it is concluded that the non-uniform inflow generated by channel head leads to the outflow of the pump differing from the straight pipe inflow.

To clearly clarify the non-uniform inflow and the difference of outflow, the lines across the center of the circle in Section Inlet and Section Outlet are selected to compare the difference of the axial velocity with different inflows, as shown in Fig. 6. The code  $r$  represents the position on the line, and  $r$  ranges from  $-0.1$  m to  $0.1$  m. Fig. 9 shows the axial velocity of the line on Section Inlet when the pump suction is respectively connected with the channel head and straight pipe at different flow rates. It is observed that both of inlet velocities of two connection styles increase with the flow rate increasing from  $0.6Q$  to  $1.2Q$ . The velocity of the line is non-uniform with  $r$  ranging from  $-0.1$  m to  $0.1$  m when the pump suction is connected with the channel head. Conversely, the velocity of the line is uniform with  $r$  ranging from  $-0.1$  m to  $0.1$  m when the pump suction is connected with the straight pipe. Fig. 10 shows the axial velocity of the line on Section Outlet when the pump suction is respectively connected with the channel head and straight pipe at different flow rates. It is observed that both of outlet velocities of two connection styles increase with the flow rate increasing from  $0.6Q$  to  $1.2Q$ . However, the outflow pattern changes when the pump suction is connected with the channel head, the velocity of

the line on the Section Outlet changes more gentle, especially at 0.6Q flow rate. Conversely, when the pump suction is connected with the straight pump, the velocity of the line on the Section Outlet varies intensely. The velocity is negative at part of the line, which also could be observed in Fig. 8(b). It means the backflow occurs at the outlet, and the backflow blocks partial of the flow passage, which leads to the velocity of other part higher.

In conclusion, the non-uniform inflow has a great effect on the flow structures in the pump, and it leads to the outflow different from that of the straight pipe. So it is sorely necessary to investigate the unsteady hydraulic dynamic characteristics of the pumps with non-uniform inflow by experiment method.

### 3.2. Unsteady pressure pulsation of the model pump with Non-uniform inflow

The pressure pulsations in the casing and outlet pipe are important input conditions for the design of the nuclear reactor. To evaluate pressure pulsation energy in particular frequency band, Root Mean Square (RMS) method is applied to deal with discrete pressure signals, as presented in Eq. (1) and Eq. (2),

$$RMS = \sqrt{\frac{1}{n} \sum_{i=1}^n (A_i - \bar{A})^2} \quad (1)$$

$$\bar{A} = \frac{1}{n} \sum_{i=1}^n A_i \quad (2)$$

where  $A_i = \Delta H/H$  represents pressure amplitudes at different frequencies, and  $\bar{A}$  is the mean amplitude. The pressure fluctuations are defined based on the peak to peak change  $\Delta H/H$ , where  $\Delta H = \Delta p/\rho g$ ,  $\Delta p = p - \bar{A}$ ,  $\bar{A}$  is the mean amplitude of the pressure,  $H$  is the head for the pump at design condition. The pressure fluctuations for the seven monitoring points are analysed using the fast Fourier transform (FFT) to obtain pressure spectrum characteristics.

Fig. 11 shows the time history of unsteady pressure pulsation signals of sensor P4 at four typical flow rates. It is observed that pressure signals fluctuate obviously. From the comparison of pressure pulsations at different flow rates, it is found that the pressure pulsation amplitude at low flow rate, especially at 0.2Q, is much larger than that at nominal flow rate. This situation is connected with the flow separation structure in the model pump, such as the rotating stall phenomenon in the flow passage.

To investigate the pressure pulsation characteristics at different flow rates and measuring positions, frequency spectra at sensor P4 and P7 are shown in Fig. 12 at four flow rates, namely 0.2Q, 0.6Q, 1.0Q and 1.2Q. It has been generally accepted that rotor-stator interaction is a primary reason for high amplitude pressure pulsation in pumps. Two basic frequencies caused by rotor-stator interaction are the excitation of the stator flow at  $f_{SPF}$  and the excitation of the rotor flow at  $f_{RPF}$ . The rotating frequency of impeller blade  $f_R$  and its higher harmonics  $2f_R$ ,  $3f_R$ , and so on are also expected. As observed,  $f_{RPF}$  has the maximum amplitude at 0.2Q, 0.6Q and 1.0Q. Generally, amplitudes at  $f_{RPF}$  are higher than that at other frequencies. However, there are noticeable peaks at  $2f_R$ ,  $3f_R$ , and the harmonics of  $f_R$  at conditions of 0.2Q, 0.6Q, 1.0Q and 1.2Q.  $f_R$  reaches the maximum amplitude at 1.2Q. This excitation may be caused by circumferential non-uniformities in the flow which might be generated by the volute (Brennen, 2011). It is concluded that  $f_{RPF}$  is not always the dominant frequency, and its magnitude is often less than the other frequencies. The stator frequency  $f_{SPF}$  and its higher harmonics  $2f_{SPF}$  also occur at 0.2Q, 0.6Q, 1.0Q and 1.2Q, but for P4 and P7 at 1.2Q, it is difficult to identify discrete peaks at  $2f_{SPF}$ . Apart from the above  $f_{SPF}$ ,  $f_{RPF}$ ,  $f_R$  and its higher harmonics, subharmonics generated by nonlinear interaction could

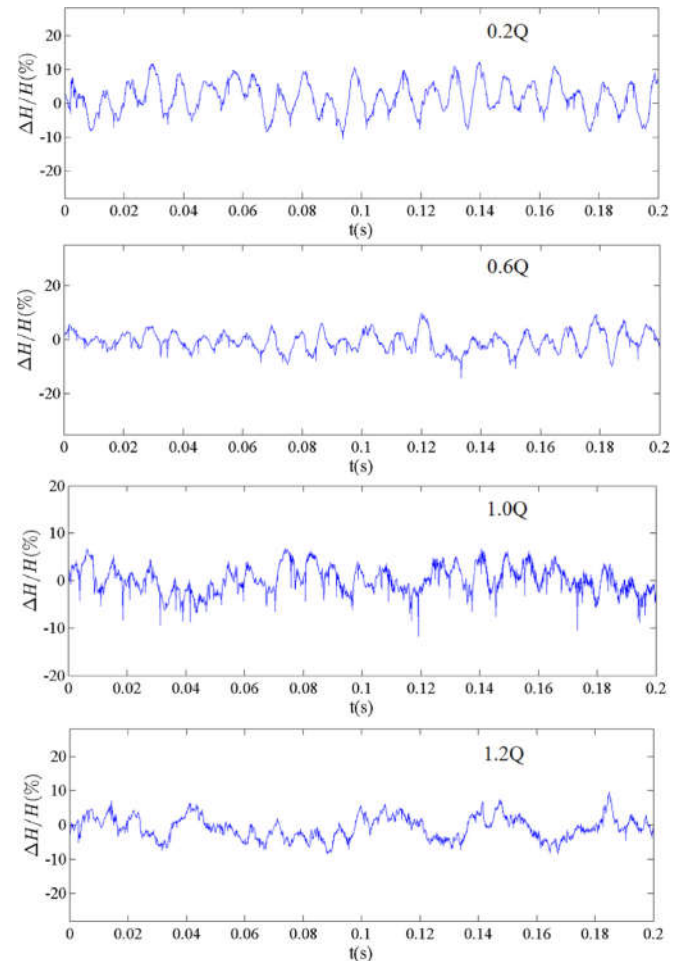
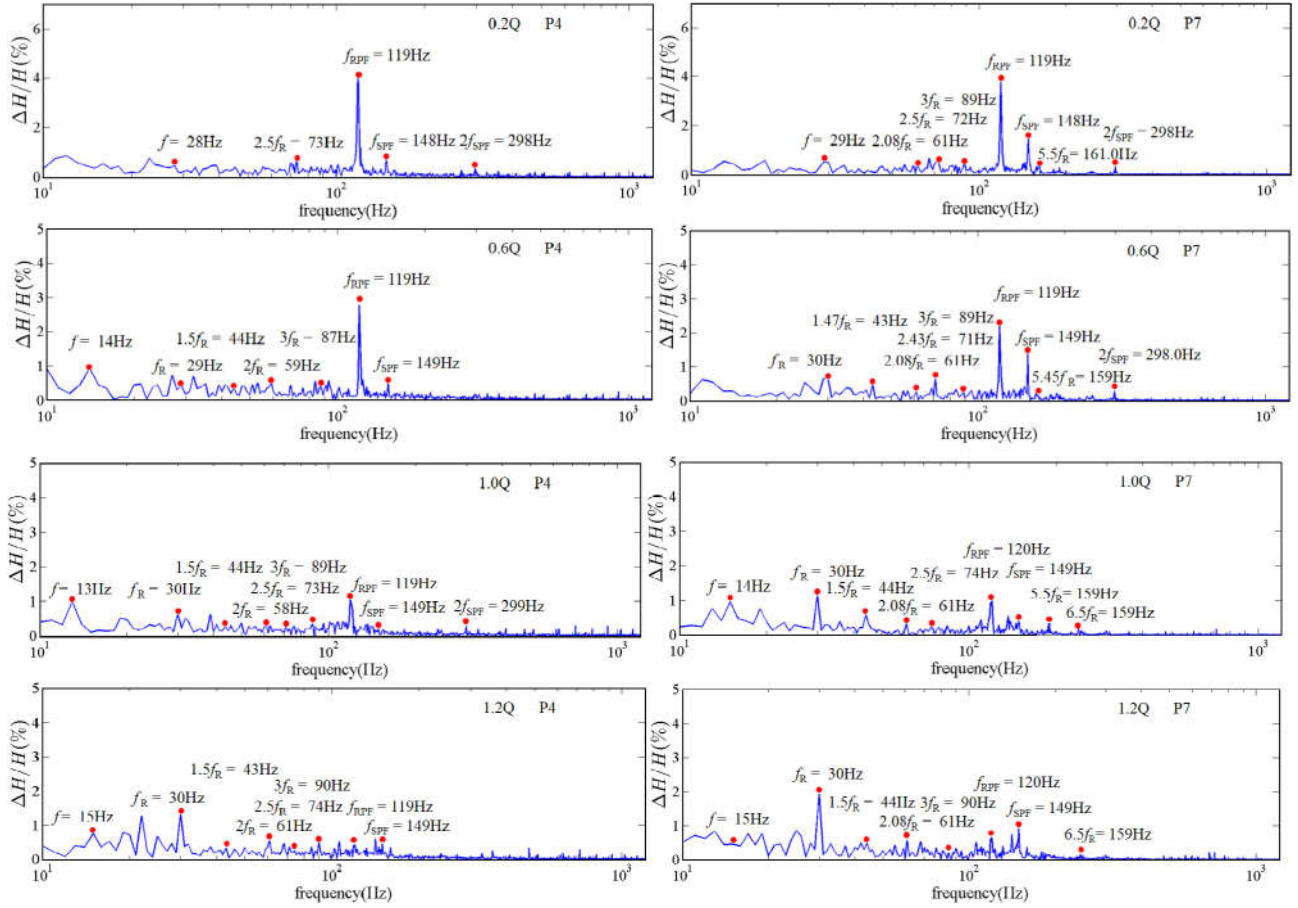


Fig. 11. Unsteady pressure signals of sensor P4 at four typical flow rates.

also be observed. It is notable that at some operating conditions, the amplitudes are distinct at component  $0.5f_R$ , such as 13 Hz to 15 Hz, which are probably caused by secondary flow in the pump. Rotor shaft displacement signals in real time are measured by the eddy current sensors, which are equipped in upper end of the upper bearing and lower end of the lower bearing. The shaft displacement signals are analysed by FFT method, and it appeared half  $f_R$  frequency whirl in the spectrum. There may be a certain relationship between the pressure pulsation and shaft displacement at  $0.5f_R$  component.

As illustrated in Fig. 12, pressure amplitude at  $f_R$  increases with flow rate increasing, it is difficult to identify the discrete peaks at low flow rates, and the discrete peaks at high flow rates are obvious. With an opposite tendency relative to  $f_R$ , the pressure amplitude at  $f_{RPF}$  decreases rapidly with flow rate increasing, and it is even less than the pressure amplitude at  $f_R$  at 1.2Q flow rate. Meanwhile, it is easy to find that different measuring positions also have an effect on the pressure spectrum. At 1.0Q, predominant component corresponds to  $f_{RPF}$  at p4, but predominant component corresponds to  $f_R$  at p7. In this situation, the magnitude at  $f_{RPF}$  is smaller than other frequencies, and this is because nonlinear interaction components lower the  $f_{RPF}$  intensity leading to their distribution of energy at  $f_{RPF}$  among other higher harmonics. As shown in Fig. 12, there are a number of nonlinear components generated due to nonlinear interaction between  $f_R$  and  $f_{RPF}$ . The nonlinear components have the form of  $0.5mf_R$ , where m is integer.

In order to investigate the relationship between pressure pulsation energy and flow rate, Fig. 13 presents RMS values of different



**Fig. 12.** Pressure spectra of pressure sensors P4 and P7 at different flow rates.

pressure transducers at different flow rates. As illustrated in Fig. 13, both the position of pressure transducer and the flow rate have a great effect on the RMS. In Fig. 13(a), RMS values of different pressure sensors at P1–P4 in the volute are presented. The pressure pulsation energy reaches a minimum level when the model pump operates near nominal flow rate. Pressure sensors P1 and P2 have the similar varying tendencies, and RMS values increase first, then experience a local maximum value around 0.4Q, finally fall as flow rate increases. Pressure sensors P3 and P4 also have the similar variation tendencies, and RMS values decrease as flow rate increases. At high flow rates, RMS values at P2 and P3 increase rapidly, but RMS values at P1 and P4 increase slowly. Generally, unsteady flow phenomena would be easy to develop inside the impeller passage at off-design conditions. These unsteady flows are characterized by flow separation from blade suction side, vortex shedding at the trailing edge of the impeller, which would result in a sharp increase of pressure pulsation energy (Zhang et al., 2015). Also it is remarkable that RMS values have apparent difference at different sensors, especially at 0.5Q, RMS value of P1 is almost 2.18 times of its counterpart associated with P4, and RMS value of P3 is almost 2.46 times of its counterpart associated with P4 at 1.2Q.

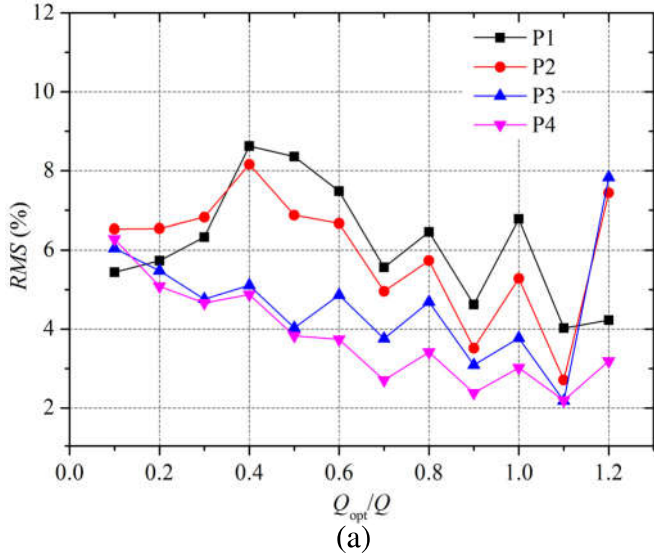
As illustrated in Fig. 13(b), RMS values of different pressure sensors at P5–P7 in the discharging pipe are presented. RMS values of different pressure sensors almost have the similar varying tendency. RMS values decrease first, then experience a local minimum value near nominal flow rate, and increase rapidly at high flow rate. The difference of RMS values between P5 and P7 is very little. However, it is noted that RMS values have apparent difference at sensor P6 compared with P5 and P7. And with the flow rate

decreasing, the difference increases. From the above analysis, it is evident that pressure fluctuation characteristics are different for various positions of the model pump with the channel head.

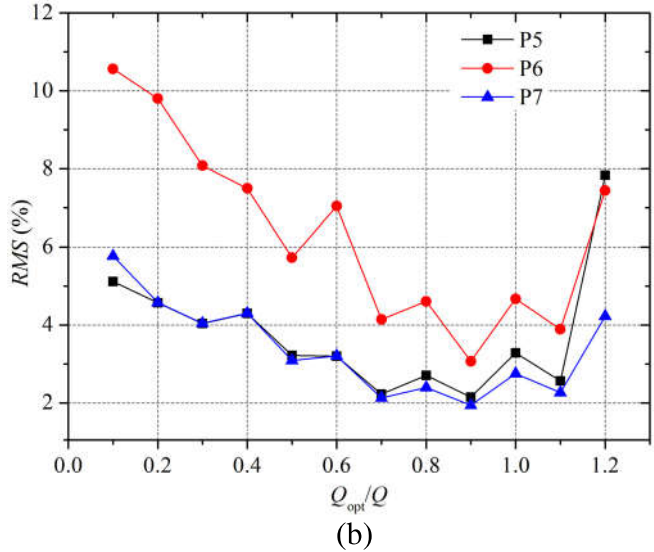
As illustrated in Fig. 12, some evident peaks are marked particularly in pressure spectrum of sensor P4 and P7 at given flow rate, and Fig. 14 shows three distinct peaks at rotating frequency  $f_R$ , rotor passing frequency  $f_{RPF}$  and stator passing frequency  $f_{SPF}$  versus flow rate. It is noted that pressure amplitudes of sensor P1–P4 at  $f_R$  fluctuate slightly for whole flow rates. Pressure amplitudes of sensor P5–P7 at  $f_R$  also fluctuate slightly at flow rates lower than 0.8Q, but at high flow rates ( $Q_{opt} > 0.8Q$ ), pressure amplitude at  $f_R$  increases gradually. Pressure amplitudes of sensor P1–P4 at  $f_{RPF}$  decrease gradually as the flow rate increases. Pressure amplitudes of sensor P5–P7 at  $f_{RPF}$  fluctuate slightly at flow rates higher than 0.8Q, but at low flow rates ( $Q_{opt} < 0.8Q$ ), pressure amplitudes at  $f_{RPF}$  increase gradually as the flow rate decreases. Furthermore, pressure amplitudes of sensor P5 and P7 fluctuate slightly when the flow rate is than 0.4Q. Pressure amplitudes of sensor P1–P7 at  $f_{SPF}$  decrease first, then experience a local minimum value near nominal flow rate, and increase gradually at high flow rate. Pressure amplitudes at  $f_R$  show the contrary trend compared with  $f_{RPF}$  and  $f_{SPF}$ . The reason is probably that energy increase at  $f_R$  is at the expense of energy decrease at  $f_{RPF}$  and  $f_{SPF}$ .

### 3.3. Influence of rotational speed on pressure pulsation characteristics of the model pump with non-uniform inflow

In the reactor coolant pump, strong rotor–stator interaction, together with intense pressure pulsation, is excited as the impeller blades pass the diffuser blades successively. So pressure pulsation



(a)

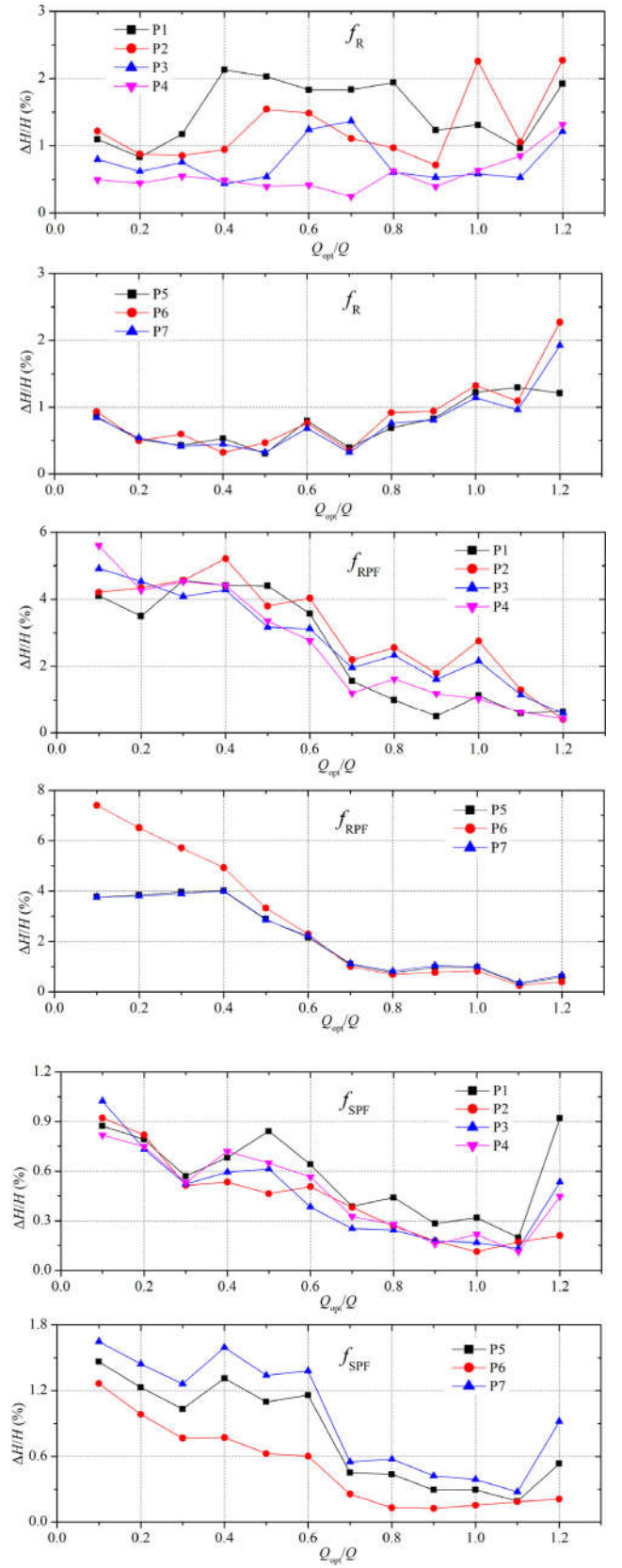


(b)

**Fig. 13.** RMS trends of different measuring points versus flow rate.

characteristics, such as the pressure amplitude of discrete component and energy distribution in particular frequency band are closely associated with the rotational speed of the impeller (Stel et al., 2013). As showed in Fig. 15, when the model pump operates at nominal flow rate, pressure spectra of P4 are presented at three rotational speeds respectively, namely 1500 r/min, 1800 r/min, and 2100 r/min. When rotating speed is 1500 r/min, peaks at  $f_R$  dominate pressure spectra at P4, and  $f_{RPF}$  is the second dominant frequency. Apart from the above  $f_{RPF}$  and  $f_R$ ,  $2f_{SPF}$  also occurs. At nominal rotational speed of 1800 r/min, some discrete peaks corresponding to  $f_R$ ,  $f_{RPF}$ ,  $f_{SPF}$  and their harmonic frequencies could be identified, and  $f_{RPF}$  is the dominant frequency. When rotating speed increases to 2100 r/min, amplitudes at  $f_{RPF}$  increase evidently. Due to the nonlinear interaction between  $f_R$  and  $f_{RPF}$ ,  $f_R$ , the nonlinear components would be generated, such as  $f_{RPF} + 3f_R$  and  $2f_{RPF} + 3f_R$ . However the component at  $f_{SPF}$  could not be identified easily.

In Fig. 16, when the model pump operates at nominal flow rate, pressure spectra of P6 are presented at three rotating speeds. When the rotating speed is 1500 r/min, peaks at  $f_{SPF}$  dominate pressure spectra at P6, and  $f_{RPF}$  is the second dominant frequency. Between  $f_{RPF}$  and  $f_{SPF}$ , nonlinear harmonics occur. At nominal rotating speed of 1800 r/min, some discrete peaks corresponding to  $f_R$ ,

**Fig. 14.** Pressure amplitudes at distinct peaks  $f_R$ ,  $f_{RPF}$  and  $f_{SPF}$  versus flow rate.

$f_{RPF}$ ,  $f_{SPF}$  and their harmonic frequencies could be identified, but the dominant frequency is 79 Hz, and  $f_R$  is the second dominant frequency. When the rotational speed increases to 2100 r/min,

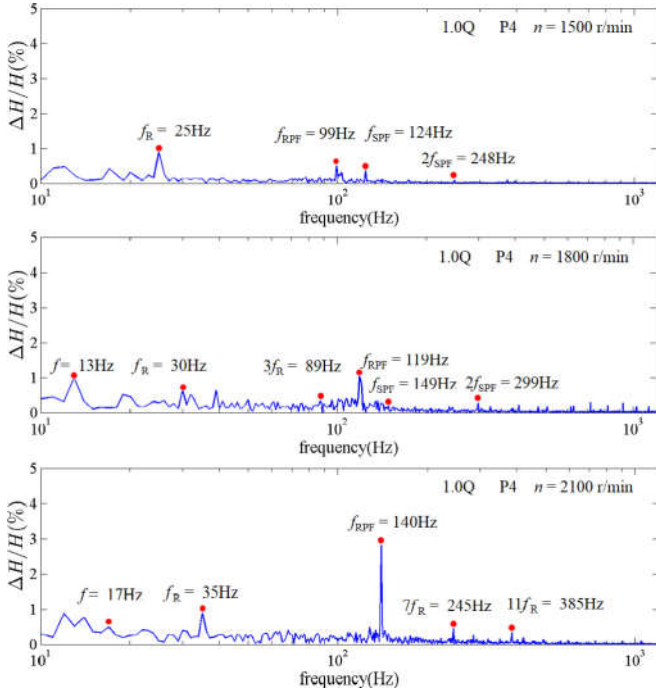


Fig. 15. Pressure spectra of P4 at three rotational speeds under nominal flow rate.

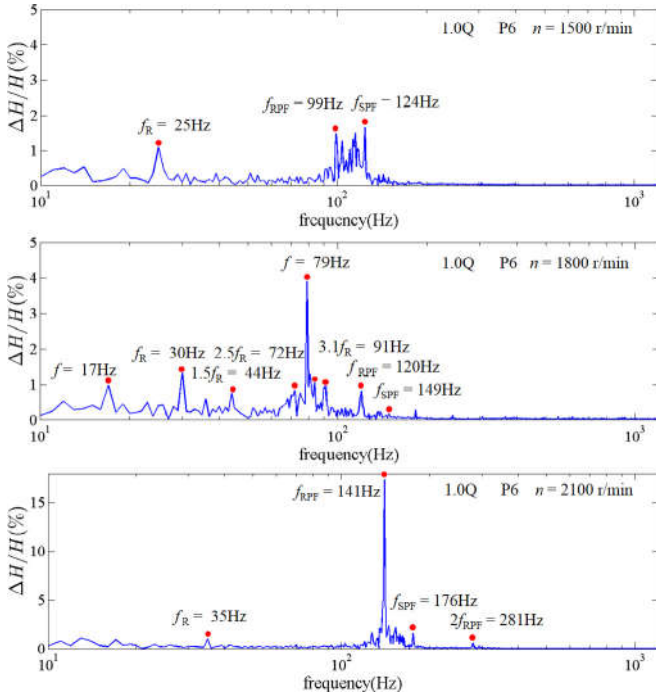


Fig. 16. Pressure spectra of P6 at three rotational speeds under nominal flow rate.

the amplitude at  $f_{RPF}$  increases evidently, and  $f_{RPF}$  is the dominant frequency. Other components like  $f_R$ ,  $f_{SPF}$  and  $2f_{SPF}$  could be identified easily. Fig. 17 shows the pressure spectra of P7 at three rotating speeds under nominal flow rate. When rotating speed is 1500 r/min, peaks at 71–74 Hz dominate pressure spectra at P7, and  $f_R$  is the second dominant frequency. The components of  $f_{SPF}$  and  $2f_{SPF}$  could be identified, but the amplitudes are weaken. At nominal rotating speed of 1800 r/min, some discrete peaks corresponding to  $f_R$ ,  $f_{RPF}$ ,  $f_{SPF}$  and their harmonic frequencies can be identified,

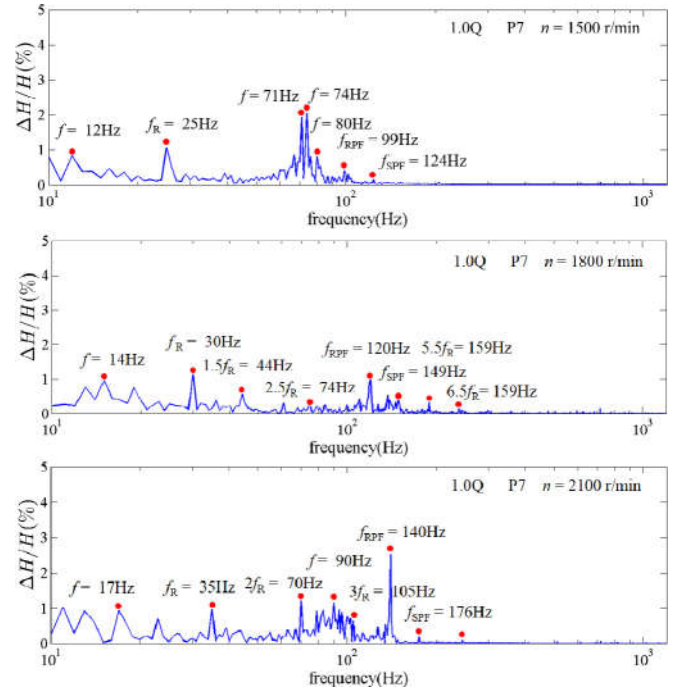


Fig. 17. Pressure spectra of P7 at three rotational speeds under nominal flow rate.

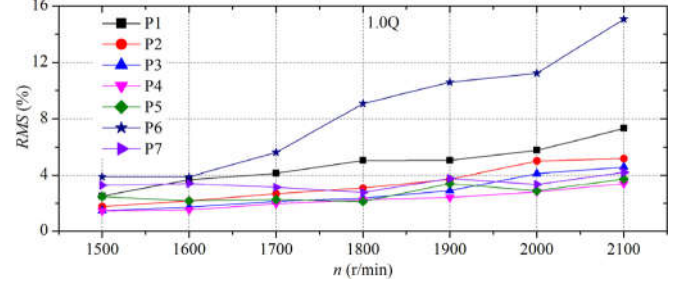
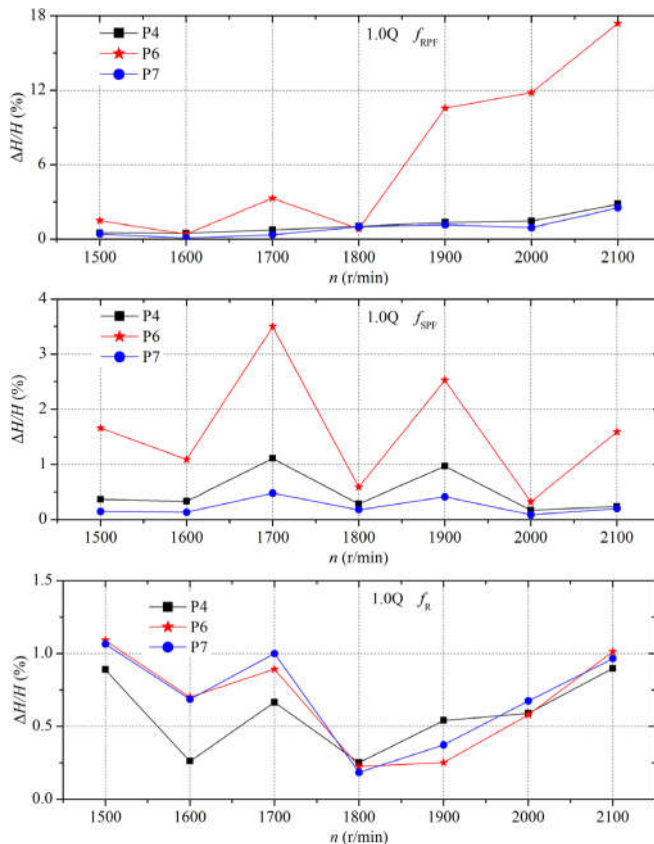


Fig. 18. Influence of rotating speed on RMS at nominal flow rate.

and  $f_R$  is the dominant frequency. When rotational speed increases to 2100 r/min, the amplitude at  $f_{RPF}$  increases evidently, and  $f_{RPF}$  is the dominant frequency obviously. Other components like  $f_R$  and its higher harmonics, as well as  $f_{SPF}$  and  $2f_{SPF}$  could be identified easily. Between  $f_R$  and  $f_{RPF}$ , nonlinear components near the frequency 90 Hz occur.

For the model pump operating at different rotating speeds, Fig. 18 shows RMS values of different measuring points for three flow rates. It is seen that RMS value increases as rotating speed increases. At nominal flow rate, from 1200 r/min to 2100 r/min, RMS value has an increment of 192.6% at P1, 195.2% at P2, 214.9% at P3, 134.7% at P4, 52.7% at P5, 286.3% at P6 and 28% at P7.

As illustrated in Figs. 15–17, some evident peaks are marked particularly in pressure spectrum of sensor P4, P6 and P7 with different rotating speeds at given flow rate, and Fig. 19 shows peaks at rotor passing frequency  $f_{RPF}$ , stator passing frequency  $f_{SPF}$  and rotating frequency of impeller blade  $f_R$  at nominal flow rate. At rotor passing frequency  $f_{RPF}$ , it is noted that pressure amplitudes of sensor P4 and P7 fluctuate slightly for whole rotating speeds. Pressure amplitudes of sensor P6 also fluctuate slightly at the rotating speeds lower than 1800 r/min, but at high rotating speeds, pressure amplitudes at  $f_{RPF}$  increase rapidly. When the rotating speed is higher than 1800 r/min, pressure amplitudes of sensor P6 at  $f_{RPF}$  are larger than other sensors. At stator passing frequency



**Fig. 19.** Influence of rotating speed on pressure amplitudes at distinct peaks  $f_{RPF}$ ,  $f_{SPF}$ , and  $f_R$ .

$f_{SPF}$ , it is noted that pressure amplitudes of sensor P4 and P7 fluctuate slightly at whole rotating speed, but pressure amplitude of sensor P6 fluctuates acutely. The pressure amplitude of sensor P6 has a maximum value at 1700 r/min at nominal flow rate. At rotating frequency of impeller blade  $f_R$ , pressure amplitudes of sensor P4, P6 and P7 decrease slowly, and they have minimum values at 1800 r/min, then increase gradually with the rotating speed increasing.

#### 3.4. Discussion

From the analysis of flow structures at inlet and outlet, we can find that the non-uniform inflow has a great effect on the flow structures within the pump, and the research on the unsteady flow of the model pump with different inflow would be conducted by experiment method. And the inlet flow structure should be visualised by advanced measurement method. As shown in Figs. 16–19, pressure pulsation energy at sensor P6 is higher and acute, and the nonlinear components of sensor P6 can be identified easily. The reason maybe that the vortex near P6 makes the redistribution of the pressure pulsation energy for the nonlinear interaction. And more detailed analysis of the flow field near P6 would be carried out. Through analysis of the influence of rotating speed on pressure pulsation, we can find that when the rotating speed increases, pressure pulsation energy decreases. So it is an effective measure to reduce vibration energy by adjusting rotational speed of the impeller.

#### 4. Conclusion

Compared with uniform inflow, at low flow rates ( $Q_{opt} < 0.5Q$ ), the head of the pump with non-uniform inflow increases with

the flow rate decreasing, and the head of the pump with uniform inflow has an opposite trend, and at the nominal flow rate, the head of the pump with non-uniform inflow decreases by 0.46%, the efficiency of the pump with non-uniform inflow decreases by 7.5%, and the power of the pump with non-uniform inflow increases by 7.32%. In conclusion, non-uniform inflow has a great effect on the pump performance.

From the analysis of flow field in the pump with different inflows, the non-uniform inflow has a great effect on the flow structures in the pump, so unsteady pressure pulsation characteristics in reactor coolant pump with channel head are investigated by experiment method. Pressure pulsation signals measured from the sensors on the pump casing and outlet pipe are analysed by FFT and RMS method. Pressure fluctuation characteristics, both discrete peaks and RMS values, are easily affected by different operating conditions and measuring positions. Pressure amplitudes at  $f_{RPF}$  and  $f_{SPF}$  decrease with flow rate increasing, but pressure amplitudes at  $f_R$  present the contrary trend.

Meanwhile, the effect of rotating speed on pressure pulsation is analysed. It is found that pressure amplitudes of RMS value and  $f_{RPF}$  increase with rotating speed increasing. In general, low rotating speed will reduce the pump vibration, so adjusting rotating speed is an appropriate method to stable operation of the pump. Nonlinear frequency components of sensor P6 can be identified easily, and more detailed analysis of the flow field near P6 would be carried out.

Finally, it is expected that the present work will provide a different view considering non-uniform inflow in design of the pump and a deep analysis on pressure pulsation. In further study, comparative study on the pressure pulsations in the reactor coolant pump with channel head and straight pipe will be conducted by experimental method, and flow field of the inlet will be measured by PIV as well.

#### Acknowledgments

This work is funded by Shanghai Economy Information Technology Committee – China (15GFZ-GB02-060) and National Natural Science Foundation of China – China (No. 51576125).

#### References

- Barrio, R., Blanco, E., Parrondo, J., González-Alejo, J., Fernández-Andez, J., 2008. The effect of impeller cutback on the fluid-dynamic pulsations and load at the blade-passing frequency in a centrifugal pump. ASME J. Fluids Eng. 130, 111102.
- Barrio, R., Parrondo, J., Blanco, E., 2010. Numerical analysis of the unsteady flow in the near-tongue region in a volute-type centrifugal pump for different operating points. Comput. Fluids 39, 859–870.
- Benra, F.-K., 2006. Numerical and experimental investigation on the flow induced oscillations of a single-blade pump impeller. ASME J. Fluids Eng. 128, 783–793.
- Brennen, C.E., 2011. Hydrodynamics of Pumps. Cambridge University Press.
- Cheng, H., Li, H., Yin, J., Gu, X., Hu, Y., Wang, D., 2014. Investigation of the distortion suction flow on the performance of the canned nuclear coolant pump, In: Conference: ISFMFE2014, At Wuhan, China.
- Cheong, J.-S., 2000. An analytical prediction on the pump-induced pressure pulsation in a pressurized water reactor. Ann. Nucl. Energy 27, 1373–1383.
- Huang, W., Zhang, W.-Q., Tao, W.-Q., He, J.-S., Huang, H., Zhang, F.-Y., Liu, X.-B., 2002. Flow characteristics experimental study within connection between steam generator channel head and pump suction. Nucl Power Eng 23, 38–42.
- Lee, K.B., Im, I.Y., Lee, S.K., 1992. Analytical prediction on the pump-induced pulsating pressure in a reactor coolant pipe. Int. J. Press. Vessels Pip. 52, 417–425.
- Lee, L., Chandra, S., 1980. Pump-induced fluctuating pressure in a reactor coolant pipe. Int. J. Press. Vessels Pip. 8, 407–417.
- Li, D., Gong, R., Wang, H., Xiang, G., Wei, X., Liu, Z., 2015. Dynamic analysis on pressure fluctuation in vaneless region of a pump turbine. Sci China Technol Sci 58, 813–824.
- Parrondo-Gayo, J.L., Gonzalez-Perez, J., Fernández-Franco, J.N., 2002. The effect of the operating point on the pressure fluctuations at the blade passage frequency in the volute of a centrifugal pump. ASME J. Fluids Eng. 124, 784–790.
- Pei, J., Yuan, S., Benra, F.-K., Dohmen, H.J., 2012. Numerical prediction of unsteady pressure field within the whole flow passage of a radial single-blade pump. ASME J. Fluids Eng. 134, 101103.

- Pei, J., Yuan, S., Yuan, J., 2013. Numerical analysis of periodic flow unsteadiness in a single-blade centrifugal pump. *Sci China Technol Sci* 56, 212–221.
- Penzes, L., 1974. Theory of pump-induced pulsating coolant pressure in pressurized water reactors. *Nucl. Eng. Des.* 27, 176–188.
- Spence, R., Amaral-Teixeira, J., 2009. A CFD parametric study of geometrical variations on the pressure pulsations and performance characteristics of a centrifugal pump. *Comput. Fluids* 38, 1243–1257.
- Stel, H., Amaral, G., Negrao, C., Chiva, S., Estevam, V., Morales, R., 2013. Numerical analysis of the fluid flow in the first stage of a two-stage centrifugal pump with a vaned diffuser. *J. Fluids Eng.* 135, 071104.
- Sun, H.-H., Cheng, P.-D., Miao, H.-X., 2010. *The Third Generation of Nuclear Power Technology AP1000*. China Electric Power Press, Beijing.
- Toussaint, M., 2006. Analysis of unsteady flow in centrifugal pump at off-design point operation. In: Proceeding of 23rd IAHR Symposium on Hydraulic Machinery and Systems, Yokohama, Japan, Paper.
- Van Esch, B., 2009. Performance and radial loading of a mixed-flow pump under non-uniform suction flow. *ASME J. Fluids Eng.* 131, 051101.
- Wang, H., Tsukamoto, H., 2003. Experimental and numerical study of unsteady flow in a diffuser pump at off-design conditions. *ASME J. Fluids Eng.* 125, 767–778.
- Xu, Z., Yi, F., Liu, S., Wu, Y., 2005. 2D PIV experiments on non-uniform flow in a rectangular open model pump suction passage. *ASME 2005 International Mechanical Engineering Congress and Exposition*. American Society of Mechanical Engineers, pp. 523–530.
- Yang, S.-S., Kong, F.-Y., Chen, H., Su, X.-H., 2012. Effects of blade wrap angle influencing a pump as turbine. *ASME J. Fluids Eng.* 134, 061102.
- Yang, S.-S., Liu, H.-L., Kong, F.-Y., Xia, B., Tan, L.-W., 2014. Effects of the radial gap between impeller tips and volute tongue influencing the performance and pressure pulsations of pump as turbine. *ASME J. Fluids Eng.* 136, 054501.
- Yao, Z., Wang, F., Qu, L., Xiao, R., He, C., Wang, M., 2011. Experimental investigation of time-frequency characteristics of pressure fluctuations in a double-suction centrifugal pump. *ASME J. Fluids Eng.* 133, 101303.
- Zhang, N., Yang, M., Gao, B., Li, Z., Ni, D., 2015. Experimental investigation on unsteady pressure pulsation in a centrifugal pump with special slope volute. *ASME J. Fluids Eng.* 137, 061103.